#### Contents lists available at ScienceDirect

## Acta Materialia

journal homepage: www.elsevier.com/locate/actamat



Full length article

# Distinct driven steady states emerge from diverse initial textures in rolled nanocomposites



Ian Chesser<sup>a,\*</sup>, Elizabeth A. Holm<sup>a</sup>, Michael J. Demkowicz<sup>b</sup>

- <sup>a</sup> Department of Materials Science and Engineering, Carnegie Mellon University, 5000 Forbes Avenue, Pittsburgh, PA, 15213-3890, United States
- <sup>b</sup> Department of Materials Science and Engineering, Texas A&M University, College Station, TX 77845, United States

#### ARTICLE INFO

Article history: Received 24 July 2019 Revised 27 September 2019 Accepted 29 October 2019 Available online 11 November 2019

Keywords:
Nanocomposites
Interfaces
Severe plastic deformation
Rolling
Molecular dynamics

#### ABSTRACT

Severe plastic deformation is a widespread method of making high-performance metallic materials. Single-phase polycrystalline metals undergoing severe plastic deformation develop steady-state textures that are characteristic of the mode of deformation. By contrast, we show that two-phase, Cu-Nb nano-laminate composites reach a variety of different steady-state textures under a single mode of deformation. Using molecular statics simulations and a novel algorithm for crystal rotation analysis, we observe that the final, steady state texture and interface character in these materials depends on the initial texture of the composite. This finding suggests that the range of bulk Cu-Nb nano-composite textures that may be made by severe plastic deformation is larger than previously demonstrated, with multiple plastically-driven steady states accessible, depending on initial texture. We propose a modification of accumulative roll bonding with highly textured seed layers as a means of accessing different driven steady states in layered composites.

© 2019 Acta Materialia Inc. Published by Elsevier Ltd. All rights reserved.

## 1. Introduction

A polycrystalline metal is an ensemble of spatially oriented, single crystals or "grains". The distribution of grain orientations, known as texture, has long been recognized as a key factor governing the properties of polycrystals [1]. Consequently, considerable effort has gone into developing methods for controlling texture [1–3]. We use atomistic simulations to demonstrate that a much broader range of texture control is possible in multi-phase metal composites than in single-phase metal polycrystals [4].

One of the most effective approaches for modifying texture in metals is through severe plastic deformation (SPD), wherein specimens are forced to undergo extreme changes in shape through the application of external mechanical forces [5]. As a specimen is deformed, its texture changes and eventually reaches a steady-state, which is independent of the initial texture and remains invariant upon further deformation [5,6,10,14]. A wide variety of SPD methods are now commonly in use, each one giving rise to its own characteristic steady-state texture in single phase metals [4,7]. By contrast, we show that in two-phase metal composites, even a single mode of SPD gives rise to a variety of steady-state textures, depending on the initial texture of the composite.

Our investigation focuses on the response of copper(Cu)-niobium(Nb) laminate composites to SPD via accumulated roll bonding (ARB). ARB of Cu-Nb laminates has received considerable attention, as it yields exceptionally sharp textures corresponding to very narrow variations in grain orientations [6,8]. Such textures afford fine-scale control not only over grains, but also over the interfaces between grains. For example, when Cu-Nb composites are rolled down to layer thicknesses well below 1 micron, interfaces between adjacent Cu and Nb grains exhibit one predominant crystallographic character [6]. These interfaces impart multiple desirable properties to the composite, including resistance to radiation [10,11,13], high strength [12,15,16], and thermal stability [9].

The interfaces expressed during ARB have been found to vary with rolling direction and the amount of rolling [16,27]. In a variant of ARB known as cross rolling, the sample is rotated by 90° at a layer thickness of 60 nm. This rotation represents a change in strain path and leads to new steady state textures upon continued deformation [16]. At fine layer sizes less than 50 nm, twinning is observed in the Cu layer and leads to new texture components associated with the ARB Goss orientation relationship [16,43]. We propose a modification of ARB by incorporating highly textured seed layers into the composite material. One way of preparing such seed layers is by using physical vapor deposition (PVD), which results in a strong texture that is different from that formed during ARB [15]. This approach may increase the variety of steady-state

<sup>\*</sup> Corresponding author.

E-mail address: ichesser@andrew.cmu.edu (I. Chesser).

textures accessible in Cu-Nb laminates, expanding the scope for control of interface character in these materials and, consequently, of these composites' ultimate performance.

#### 2. Methods

### 2.1. Atomistic simulation of plastic deformation

To investigate texture evolution in Cu-Nb composites, we simulate high-strain plastic deformation via quasistatic loading and energy minimization of atomistic models. The advantage of this approach is that it accounts for all non-rate-dependent deformation mechanisms, including dislocation glide [18], twinning [17], and interfacial plasticity [19], at the atomic level, without making any assumptions on which mechanisms are dominant or how they interact with material microstructure and applied loads. Its drawbacks are that it only represents mechanical response in a relatively small volume; it is restricted to the "athermal limit" (T=0 K), where deformation is triggered by mechanical forces alone with no contribution from thermal activation [20]; and it does not capture rate-dependent deformation mechanisms such as dislocation entanglement. As such, it follows a quasi-static deformation path, wherein the material always remains in a local energy minimum within its configuration space, never venturing uphill to surmount an activation energy barrier. By contrast, at non-zero temperatures, departures from local energy minima do occur, leading, on occasion, to the activation of addition structural re-arrangements that do not take place in the athermal limit.

Following [34], we construct Cu-Nb bicrystal models with dimensions that minimize the misfit between the adjacent Cu and Nb layers, thereby reducing the stresses associated with the imposition of periodic boundaries. Interatomic bonding is represented using a Cu-Nb EAM potential as developed in Ref. [42]. As-constructed models are relaxed using the conjugate gradient method. Both atomic positions as well the box shape are allowed to change during this initial relaxation, yielding an initially stressfree composite model. Deformation is performed in constant increments of 0.1% initial length reduction along the ND. Volume is conserved during deformation, with expansion along the RD and no deformation along the TD. After each strain increment, the potential energy of the system is minimized, leading to rearrangement of atoms in the system to accommodate the deformation. A conjugate gradient minimization is performed in LAMMPS with force tolerance  $10^{-8}$  eV/angstrom and a relative energy tolerance  $10^{-8}$ . 900 deformation increments of equal magnitude are applied, giving a reduction of the initial layer thickness by 90% by the end of the simulation.

## 2.2. Analysis of crystal rotation

To characterize deformation-induced lattice rotations quantitatively, we use polyhedral template matching (PTM): an algorithm for determining the instantaneous orientations of the local crystal lattice surrounding individual atoms [22]. An implementation of this algorithm is freely available in the visualization software OVITO [23]. We discuss three post-processing steps required to extract orientation relationships from local atomic orientations given by PTM: symmetrization of orientations, clustering of local atomic orientations into grains, and correlation of grain orientations across interfaces.

Within a grain, orientations from PTM may be artificially banded. These bands correspond to symmetry-equivalent variants of an orientation due to the cubic point group symmetry of Cu and Nb crystals. We convert each local atomic orientation to a unique orientation by applying cubic symmetry operators and keeping the orientation that lies in the Rodrigues-Frank fundamental zone.

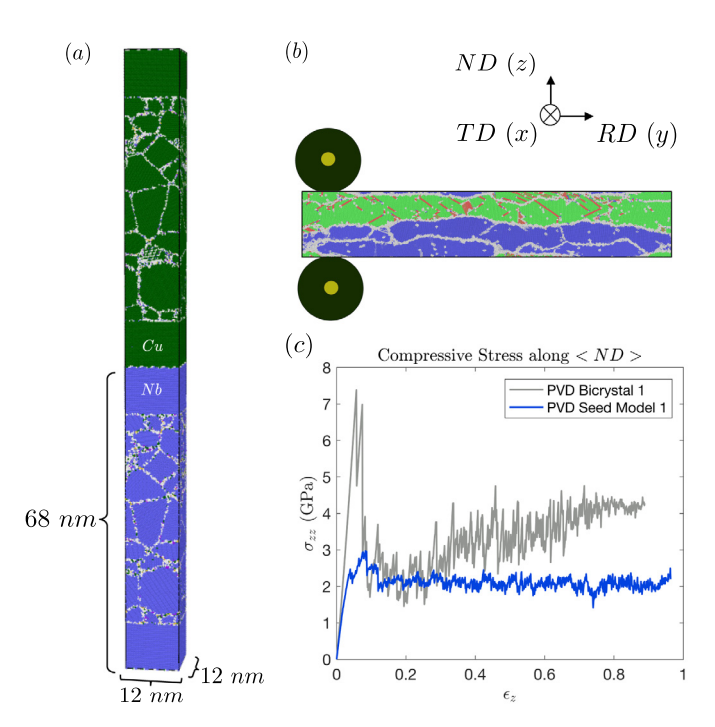


**Fig. 1.** Atomistic simulation of plastic deformation. (a) An example of an asconstructed model prior to plastic deformation. (b) The model shown in (a) after severe compression along ND and extension along RD, approximating the strain state at the mid-point of the rolled specimen. (c) Illustrative stress-strain curves obtained during deformation simulations.

After symmetrizing local orientations, we identify grain orientations at each strain step as peaks in a local orientation histogram. Peak finding is performed for 2-D histograms with two angles: the angle of the rotation axis of the orientation in stereographic projection and the scalar component of the orientation quaternion. This procedure is sufficient to identify all grains in the simulation. The size of each grain is approximated as the number of perfectly coordinated atoms contributing to each peak in an adaptively sized region of monotonic decay around the peak (a typical peak width is  $0.5^{\circ} \times 2^{\circ}$ ). This procedure yields grain orientations for all peaks and volume fractions for each orientation. Performing this analysis at each strain step gives orientation trajectories and the strength of individual texture components as a function of strain. Crystallographic directions are plotted along loading axes via stereographic projection in inverse pole figures.

Steady state orientations are matched across the Cu-Nb interface in each model at high strains. Average positions of grains are compared across the interface to determine crystallographic characters expressed at the interface.

## 3. Results

## 3.1. Simulation of mechanical deformation

Fig. 1 shows an illustrative example of our deformation simulations. The models initially consist of equal thickness Cu and Nb layers under periodic boundary conditions with interfaces between them spanning the x-y plane. Because the model is periodic in all three directions, it actually contains two Cu-Nb interfaces. We apply compression in the direction normal to the layers ("ND," parallel to the y-axis) while extending them in the rolling direction ("RD," parallel to the x-axis) such that the total volume remains constant. Model dimensions in the transverse direction ("TD," parallel to the z-axis) are held fixed. This mode of deformation—plane strain compression—mimics the plastic strain in the center

Table 1 Initial model textures.

Model	{N D}	<r d=""></r>	<t d=""></t>
PVD bicrystal 1 PVD bicrystal 2 ARB bicrystal 1 ARB bicrystal 2 random model PVD seed model 1 PVD seed model 2	Cu{1 1 1}  Nb{1 1 0} Cu{1 1 1}  Nb{1 1 0} Cu{1 1 2}  Nb{1 1 2} Cu{1 1 2}  Nb{1 1 2} Cu{1 1 2}  Nb{1 1 2} Approximately random texture PVD bi 1+random bulk layers PVD bi 2+random bulk lyers	Cu<1 1 0>  Nb<1 1 1> Cu<1 1 2>  Nb<1 1 2> Cu<1 1 0>  Nb<1 1 1> Cu<1 1 0>  Nb<1 1 1> Cu<1 1 1>  Nb<1 1 0>	CU<1 1 2>  Nb<1 1 2> Cu<1 1 0>  Nb<1 1 1> Cu<1 1 1>  Nb<1 1 1> Cu<1 1 1>  Nb<1 1 0> Cu<1 1 0>  Nb<1 1 1>

of a sample undergoing rolling. The initial layer thicknesses in our models range from 12 to 67 nm, depending on the model, and the corresponding final layer thicknesses after deformation are 2 to 5 nm (see Methods for details on atomistic modeling). For each initial texture, we only consider one initial layer thickness.

The stress-strain curves obtained from the polycrystalline simulations exhibit an initial stress overshoot to approximately 2.5–3 GPa, depending on the model, followed by rapid convergence to steady plastic flow at about 2 GPa above a total strain of 0.1. As illustrated in Fig. 1, in some models, the flow behavior is perfect plastic while others exhibit a gradual rise in flow stress corresponding to a hardening rate of ~2.5 GPa. To accommodate the applied deformation, the microstructure and defect content of the models vary dynamically throughout the simulation (see Supplementary Movies). The Cu and Nb layers nevertheless codeform, remaining continuous and distinct throughout the simulations, with no layer pinch-off and no appreciable elemental mixing. Initially flat interlayer interfaces become increasingly corrugated with straining, but continue to span the model parallel to the x-y plane.

In addition to generating plastic strains, the nucleation and propagation of crystal defects also gives rise to crystal rotation [18]. Indeed, these rotations are responsible for texture evolution in plastically deformed crystals. Moreover, as deformation progresses, non-uniform crystal rotations caused by location-dependent twin and dislocation activity may cause multiple distinct grains to rotate and coalesce into larger grains in the Cu and Nb layers. For example, the Cu and Nb layers in the simulation shown in Fig. 1 are initially polycrystalline. However, at the end of the simulation, one Cu grain spans the entire sample thickness along the rolling direction. Meanwhile, several elongated grains dominate the texture of the Nb layer. Both layers have undergone mechanically driven grain growth. In addition to grain coalescence, we also observe grain refinement in some of our simulations.

## 3.2. Analysis of texture evolution

We investigate seven atomistic models with differing initial composite textures (see Table 1). Four of them are bicrystals constructed by joining layers of single crystal Cu and Nb, one is composed of polycrystalline Cu and Nb layers with approximately equiaxed grains, and two are created by inserting a Cu-Nb bicrystal between layers of equiaxed polycrystalline Cu and Nb. Investigating the deformation response of these seven models enables us to examine the effect of initial texture on the steady-state texture that evolves under severe straining.

The bicrystal models comprise the sharpest possible class of initial textures for Cu-Nb laminates. They are chosen to correspond to the dominant texture components of nano-laminates made by physical vapor deposition (PVD) [15] and accumulative role bonding (ARB) [6]. In the PVD models, the Cu-Nb interface plane is parallel to a  $\{111\}$ -type Cu facet and a  $\{110\}$ -type Nb facet. The orientation relation (OR) is of the Kurdjumov-Sachs type [40,41], meaning that, within the interface plane, a < 110 >-type Cu direction is

parallel to a < 111 >-type Nb direction. We consider two PVD models: one where the  $< 110 >_{\text{Cu}}$  and  $< 111 >_{\text{Nb}}$  directions are aligned with the rolling direction (RD) and another where they are aligned with the transverse direction (TD). The ARB models also assume the Kurdjumov-Sachs OR, but here the interface planes are parallel to  $\{112\}$ -type facets in both Cu and Nb. Similar to the PVD case, we consider two ARB models: one in which  $< 110 >_{\text{Cu}}, < 111 >_{\text{Nb}}$  is aligned with RD and in the other with TD. The rotation separating these ARB models is equivalent to the rotation of the ARB sample imposed during cross rolling before the final rolling pass.

Models of polycrystalline Cu and Nb with randomly selected grain orientations are constructed *via* the Voronoi tessellation method [21]. These models each contain 18–20 approximately equiaxed grains, 3–12 nm in diameter. The Cu and Nb polycrystals are joined to create a polycrystalline Cu-Nb composite model. Finally, we also consider models where the nominally random initial polycrystalline texture is varied by seeding a highly-textured Cu-Nb PVD bicrystal at the Cu-Nb interface. The un-deformed model in Fig. 1 illustrates the grain structure in such a seeded polycrsytal. Note that both Cu-Nb interfaces in the model have a seed layer. We construct two such seeded models: one for each of the aforementioned PVD bicrystal orientations.

To characterize deformation-induced lattice rotations quantitatively, we use polyhedral template matching: an algorithm for determining the instantaneous orientations of the local crystal lattice surrounding individual atoms [22]. Instantaneous crystallographic orientations along ND, RD, and TD (as defined in Fig. 1) may then be represented via inverse pole figures in the standard stereographic triangle (SST). To reveal the main texture components in our models, we construct orientation distributions within the SST by binning the lattice orientations of individual atomic sites (see Methods for details on rotation analysis). We then visualize the relative strength of texture components by plotting disks in the SST with radii proportional the volume fraction of atomic sites with the corresponding local crystal orientation.

To visualize the dynamic evolution of crystal orientations as a function of applied strain, we augment the SST with an additional axis showing the model thickness. For example, Fig. 2(a) shows the deformation-induced evolution of local lattice orientations of PVD bicrystal 2 (see Table 1). The bottom of the vertical (thickness) axis corresponds to the initial model texture while the top of this axis represents the final texture of the model. The figure displays how orientation fibers along each of the loading directions wind in orientation space as the composite is plastically deformed. In this case, it shows that the texture remains sharp throughout the entire deformation process. The crystallographic orientations along the transverse direction remain essentially unaltered in both Cu and Nb layers, with total rotations of less than 1° and 7°, respectively. By contrast, the orientations along ND and RD reverse in both layers, corresponding to rotations of 20–30° in the SST.

Fig. 2(a) furthermore indicates that the texture in the simulation reaches steady state under continued deformation. To better illustrate this fact, Fig. 2(b) plots the deformation-induced variation in the angle between ND and the Cu and Nb crystallographic

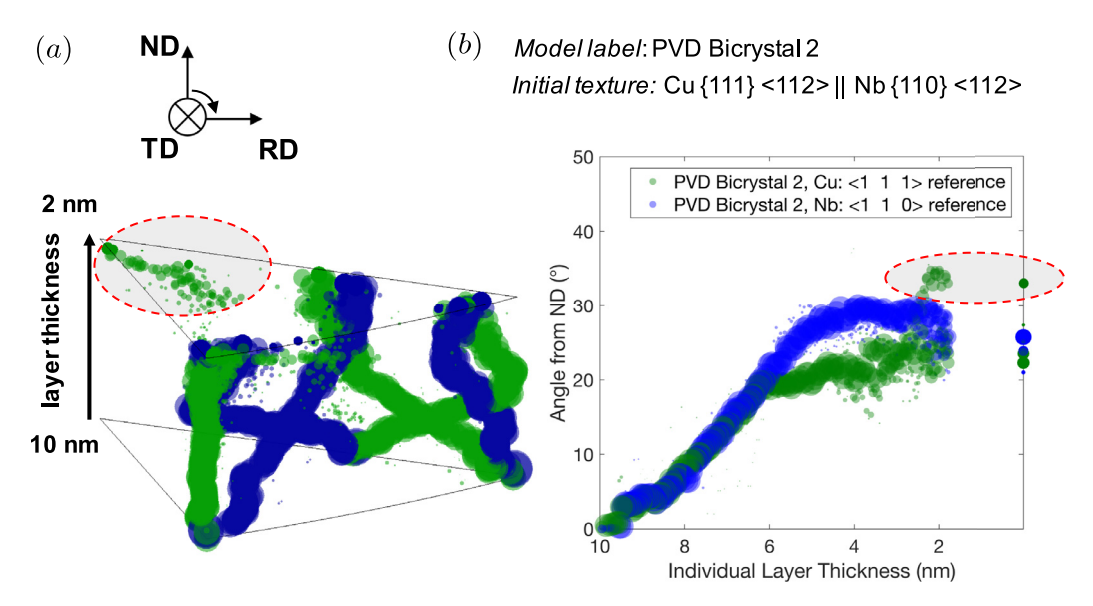


**Fig. 2.** Analysis of texture evolution in the standard stereographic triangle (SST). (a) Evolution of crystallographic directions along ND, TD, and RD for Cu (green) and Nb (blue) layers in PVD bicrystal 2 (model 2). (b) Deformation induced variation in the angle between ND and the Cu and Nb crystallographic directions initially normal to the Cu-Nb interface plane: <111> in Cu and <110> in Nb. Below a layer thickness of ~6 nm, both angles reach a steady state. The dashed ellipses in (a) and (b) indicate twin-related fibers that emerge at the end of the simulation. (For interpretation of the references to color in this figure legend, the reader is referred to the web version of this article.)

directions initially normal to the Cu-Nb interface plane: <111> in Cu and <110> in Nb. For compressive strains up to ~50%, these angles undergo a continuous, monotonic increase. However, at higher strains, they saturate and remain nearly invariant upon further deformation. The final texture in such simulations is a mechanically driven steady-state of the material. A mechanically driven steady-state is thermodynamically metastable: at elevated temperature, the system will evolve toward thermodynamic equilibrium at rates that depend on the operative kinetic processes.

All the composite models we investigated reach such driven steady states, with final textures that depend on initial texture. Our rotation analysis characterizes these steady states as well as the complex transition path connecting initial and final textures in each layer. In some models, the driven steady state consists of multiple twin-related fibers, which correspond to different points in the SST. For example, in Fig. 2(b), twinning initiates in the Cu layer when strains exceed 75% (corresponding to a layer thickness below 3 nm), stabilizing a new orientation with RD along  $\langle 001 \rangle$ . The rotation analysis in Fig. 2(a) and (b) visualizes twinning as the splitting of orientation trajectories at high strains. In the present investigation, all fibers that we know to be twin-related are considered part of the same steady-state texture. These twinned texture components in fact correspond to the well-known ARB Goss orientation relationship associated with twinning in ARB nano-composites at fine layer sizes less than 30 nm [16].

Fig. 3 compares texture evolution along the TD direction in two models with polycrystalline Cu and Nb layers: one with nominally random layer textures (model 5) and the other with an interfacial seed layer (model 6). The only difference in initial texture between these models is the seed layer in model 6, marked by a white star in Fig. 3. Both models initially have a much wider distribution of crystal orientations than the bicrystal model analyzed in Fig. 2. However, the TD trajectories in both models exhibit a clear tendency for the range of lattice orientations to decrease with deformation, consistent with grain coalescence and the eventual emergence of dominant, steady-state textures.

Closer comparison of the orientation trajectories in Fig. 3 provides direct evidence that seed layers redirect textural evolution

of the overall composite towards a different steady-state than that of the un-seeded models. In particular, the TD trajectory of the Cu layer in the seeded model pulls away from the trajectory of the Cu layer in the randomly textured model for layer thicknesses below 15 nm. For the same range of layer thicknesses surveyed in the PVD bicrystal 2 (10–4 nm), the rotations in PVD seed model 2 have already saturated. Ultimately, the textures of the Cu layers in both the seeded and un-seeded models are dominated by individual components, but the components are different in each model type. By contrast, in the Nb layers, multiple steady state orientations are present in both models.

## 3.3. Basins of attraction for deformation-induced textures

We have performed texture evolution analyses for all the models investigated in this study. Steady state Cu and Nb orientations for each model are detailed in Supplementary Table S4 and plotted along the loading direction in Fig. 4. The plastically driven steady state orientations in the PVD bicrystals (models 1 and 2) and corresponding seeded polycrystals (models 6 and 7) are largely similar. Both PVD bicrystal 2 and its seeded counterpart have major texture components with the ARB Goss OR-Cu{110}<001> || Nb {112}<110>—and minor texture components with the regular ARB OR—Cu{112}<111> || Nb {112}<110>. The regular ARB OR gives way to the ARB Goss OR at large strains with heavy twinning in the Cu layer. This behavior is consistent with experimental observations of the ARB Goss OR at layer thicknesses less than 30 nm [16]. PVD bicrystal 1 and its seeded counterpart share major texture components with Cu  $\{110\}<112> \parallel Nb \{111\}(<110> \rightarrow <112>),$ where the arrow indicates that texture along the RD in Nb is dominated by orientations distributed between <110> and <112>. The orientation trajectory connecting these directions is called the  $\gamma$ -fiber in classical literature on single crystal rolling textures [4,26], so we denote this group of ORs as ARB- $\gamma$ . PVD bicrystal 2 has additional minor texture components with variation in the Nb interface plane  $Cu\{110\}<112> || Nb (\{001\}\rightarrow\{112\})<110>$ . We label these components as the ARB- $\alpha$  OR.

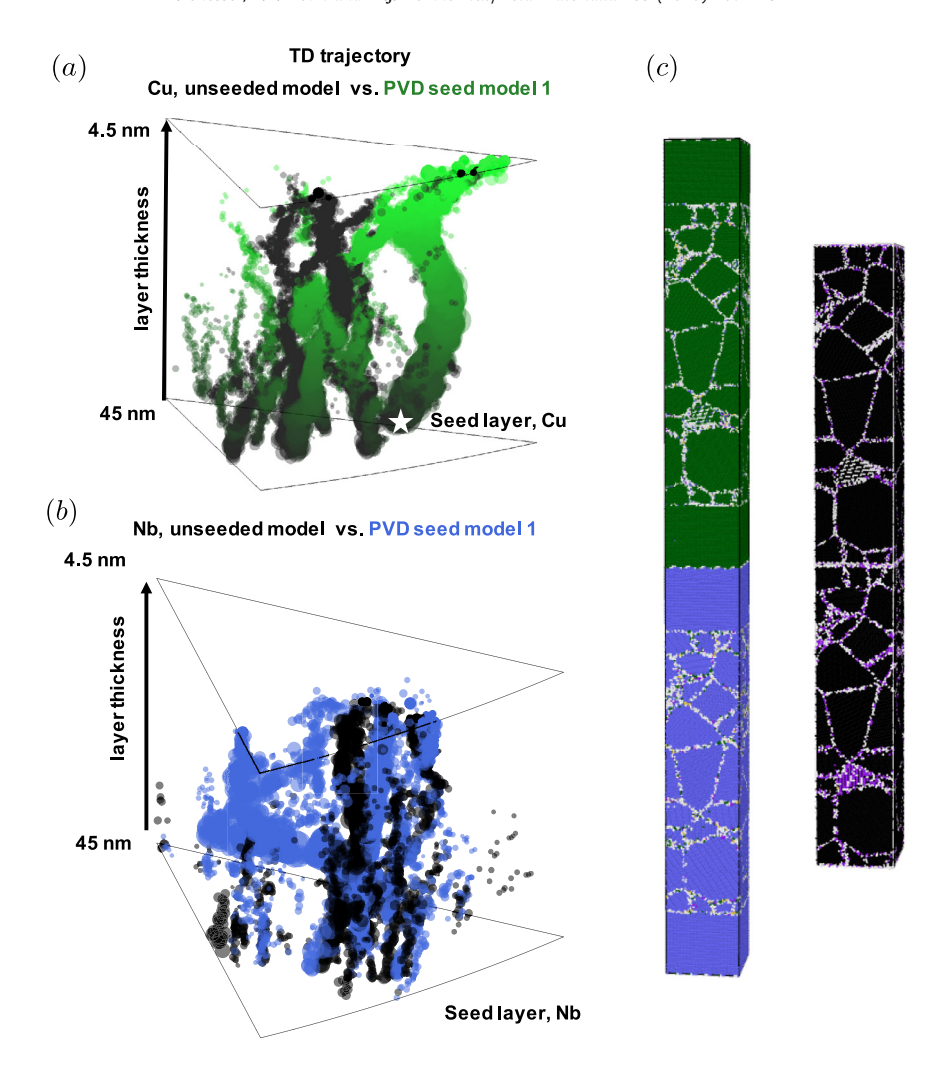


Fig. 3. Texture evolution in models with polycrystalline layers. (a) Cu layer texture in the TD. (b) Nb layer texture in the TD. (c) Atomistic models with an interfacial seed layer (left) and without one (right). In both (a) and (b), the black disks correspond to the unseeded model, also shown in black in (c). The green disks in (a) and the blue disks in (b) correspond to the seeded model in (c), with Cu and Nb layers colored green and blue, respectively. (For interpretation of the references to color in this figure legend, the reader is referred to the web version of this article.)

In contrast to the seeded models, the polycrystalline model without a seed layer does not have a single, predominant final texture component. It has three steady state texture components that fall near ARB Goss, ARB- $\gamma$ , and ARB- $\alpha$  orientation relationships. These texture components are similar to the driven steady states of the seeded models. The strengthened ARB Goss and ARB- $\gamma$  texture of the seeded models compared to the unseeded model demonstrates the influence of the seed layers during textural evolution. The ARB bicrystal models reach driven steady states corresponding to the ARB Goss OR for model 4 and a Cu({112} $\rightarrow$ {110})(<110> $\rightarrow$ <112>) || Nb {111}<112> OR for model 3. The Cu orientation of model 3 is characterized by high index crystallographic directions, but is close to the classical S texture component Cu {123}<634>.

The steady state Cu-Nb ORs detailed above define textures and orientation relations that may be accessed by varying initial texture. Moreover, because the interface planes in all of our models remain approximately parallel to the x-y plane, this data also provides the full, five-dimensional crystallographic character of the Cu-Nb interfaces, capturing both the relative rotation between the Cu and Nb crystals (three degrees of freedom) and the interface inclination (two degrees of freedom). The interface crystallographic characters (ICCs) may be represented as basins of attraction in a five dimensional space. Two basins have sharply defined ORs—ARB

and ARB Goss—while the other two represent ranges of ORs along the  $\alpha$  and  $\nu$  fibers.

We have developed a representation of the connectivity of basins of attraction in 5-D space as shown in Fig. 5. Visualizing basins of attraction is challenging because of the high dimensionality of ICC space and lack of a well-defined distance between arbitrary points in this space. These challenges are mitigated by using the recently defined octonion metric [24] to calculate distances between ICCs and by approximating the high dimensional connectivity of ICCs via dimensionality reduction [25]. Full details of this method are given in the Supplementary Information. It is found that 3 dimensions are sufficient to capture 80% of the variance in the ICC data. Although they capture information about variation in all five degrees of freedom, these dimensions may be loosely interpreted as tilt/twist angles [44].

Basins of attraction corresponding to steady state ICCs are plotted as squares in the reduced space and are colored by depth, the dimension that explains the third most variance in the high dimensional distance data. The steady state ICC data obtained from our simulations is augmented by several bicrysal ICCs (plotted as circles) culled from the experimental and crystal plasticity studies of Beyerlein et al. [6]. Lines are drawn schematically to indicate the evolution of ICCs during rolling for each model. Two main trajectories are observed in our simulations. PVD bicrystal 2 and PVD seed

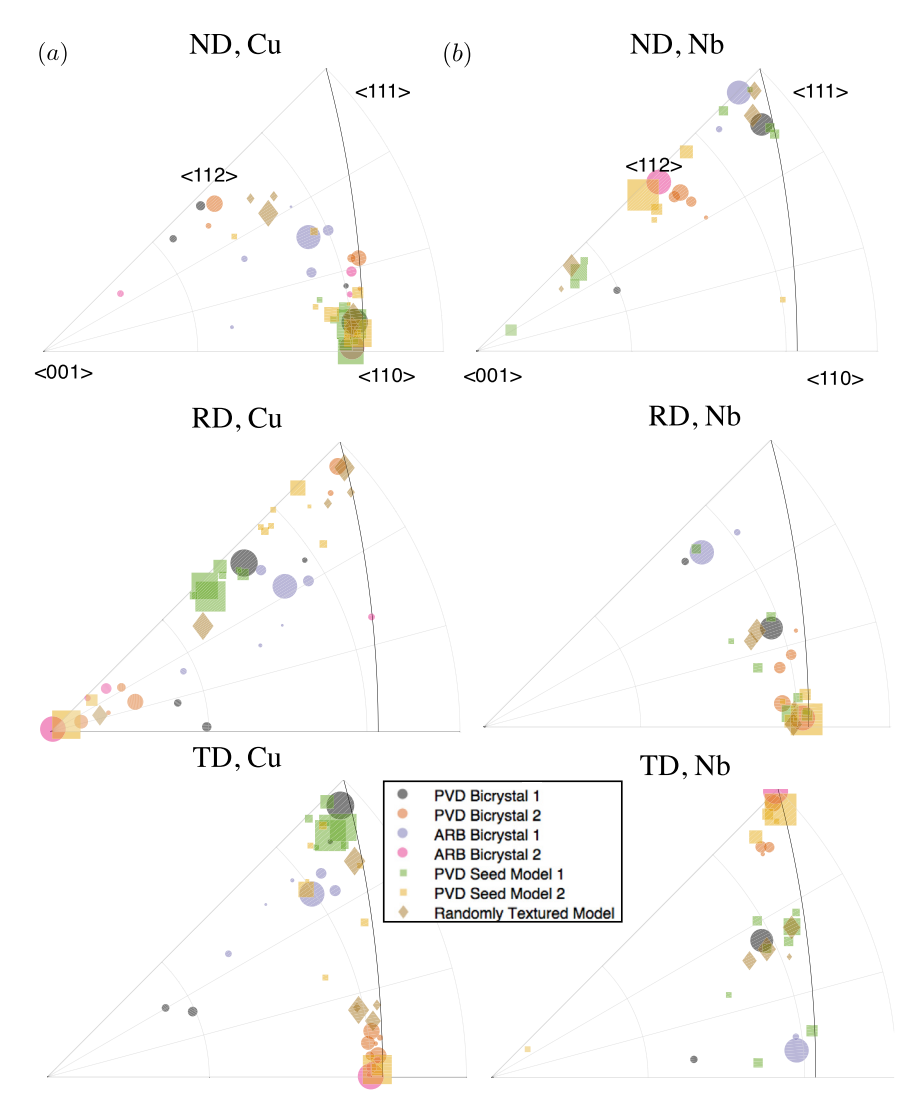


Fig. 4. Plastically driven steady state textures. (a) Driven steady states in Cu across all models along ND, TD, and RD (b) Driven steady states in Nb across all models.

model 2 both pass through the ARB and ARB Goss basins, while ARB model 1 and PVD seed model 1 pass through the ARB- $\alpha$  and  $\gamma$  basins. ARB bicrystal 2 moves from the ARB basin to the ARB Goss basin. The randomly textured model (not shown in Fig. 5) has trajectories that visit the ARB Goss, ARB- $\alpha$  and  $\gamma$  basins. Each model also has minor texture components ( $\leq$  10% volume fraction) that are not tabulated or shown in Fig. 5.

The forces that attract textures to a limited number of distinct basins are an active area of current research. One factor is interface energy. During rolling, new Cu-Nb interface area is created, incurring an energetic cost proportional to the excess energy of the interface. Low Cu-Nb interface formation energy is therefore expected to play a stabilizing role for steady-state textures under severe rolling [8]. To assess the role of interface energy in our simulations, we constructed bicrystal models with the steady-state ORs given in Fig. 5a and interface planes along the x-y plane. We then computed the energies of these interfaces and tabulated them in the Supplementary Table S5. We find that the steady-state interfaces in our models have energies in the range 1–1.2 J/m², i.e., substantially larger than interface energies in the initial PVD and ARB models of 0.55 and 0.90 J/m², respectively. The relatively high interface energies in the plastically driven states we examined imply

that steady state ORs are not only selected to minimize interface energy. Indeed, we see no evidence that low interface energy plays a role in the selection of mechanically driven steady states in these simulations.

We also analyze our modeling results in light of the plastic stability parameter developed by Beyerlein et al. to represent the capacity of bilayers to reorient under applied strain [6]. They calculated this parameter using crystal plasticity finite element (CPFE) simulations for a wide range of interfaces and reported the resulting values in Ref. [6]. A parameter value of unity indicates perfect plastic stability while zero implies rapid crystal reorientation during deformation. The interfaces found in our simulations have plastic stability parameters that range from 0.779 to 0.999, as tabulated in Supplementary Table S1. This outcome is consistent with the stability of the steady states observed in our study. However, Beyerlein et al. also predicted high plastic stability parameters for several interfaces that were not found in our models [6]. It remains to be seen whether some of them may be accessible from initial textures that were not surveyed in the present study. Supplementary Figures S1a and b correlate interface energies and plastic stability parameters to the basins of attraction identified in our simulations.

(a)	OR	$\{ND\}$	$\langle RD \rangle$	$\langle T D \rangle$
	ARB Goss	$Cu\{110\} \mid\mid Nb\{112\}$	$Cu\langle 0 0 1 \rangle \mid\mid Nb\langle 1 1 0 \rangle$	$Cu\langle 110\rangle \mid\mid Nb\langle 111\rangle$
	ARB	$Cu\{112\} \mid\mid Nb\{112\}$	$Cu\langle 111\rangle \mid\mid Nb\langle 110\rangle$	$Cu\langle 110\rangle \mid\mid Nb\langle 111\rangle$
	$ARB-\alpha$	$Cu\{110\} \mid\mid Nb\{001\} \rightarrow \{112\}$	$Cu\langle 112\rangle \mid\mid Nb\langle 110\rangle$	$Cu\langle 1 1 1 \rangle \mid\mid Nb\langle 1 1 0 \rangle \rightarrow \langle 1 1 1 \rangle$
	ARB- $\gamma$	$Cu\{110\} \mid\mid Nb\{111\}$	$\mathrm{Cu}\langle 112\rangle \    \ \mathrm{Nb}\langle 110\rangle {\rightarrow} \langle 112\rangle$	$Cu\langle 111\rangle \mid\mid Nb\langle 112\rangle \rightarrow \langle 110\rangle$

PVD bicrystal 1	90% ARB-γ
PVD bicrystal 2	60% ARB-Goss, 20% ARB
ARB bicrystal 1	80% S
ARB bicrystal 2	80% ARB-Goss
Seed model 1	70% ARB-α, 20% ARB-γ
Seed model 2	70% ARB-Goss, 20% ARB

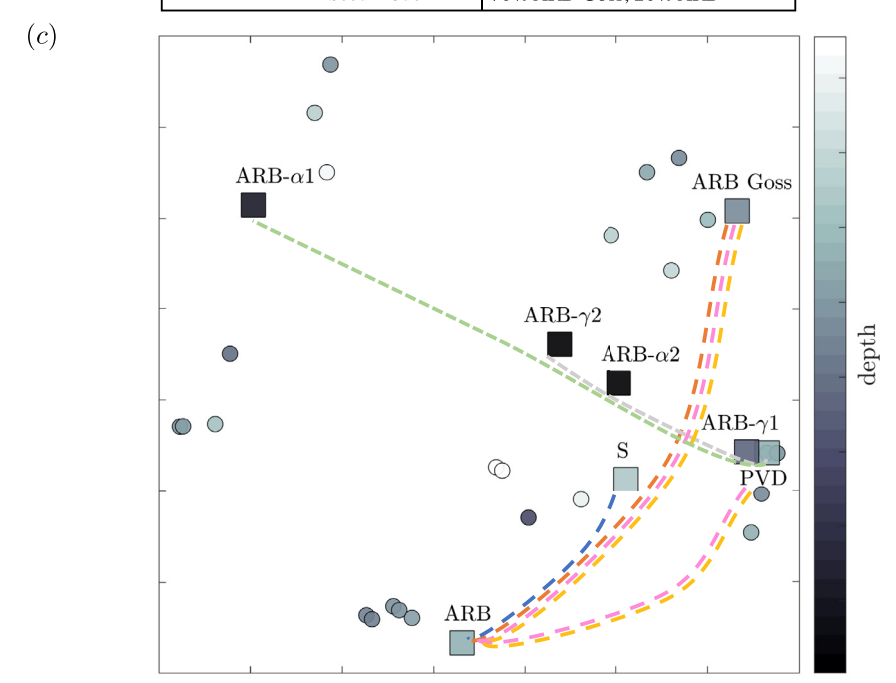


**Fig. 5.** Steady state interface crystallographic characters (ICCs). (a) Two major ICCs are ARB and ARB Goss. Other ICCs (ARB- $\alpha$ , ARB- $\gamma$ ) comprise a range of orientation relationships. (b) steady state ICCs upon deformation are tabulated for each model along with area fractions. (c) Steady state ICCs in our simulations are plotted as squares and represent basins of attraction for ICC evolution. Other points (circles) are bicrystal ICCs surveyed in CPFE simulations [6]. Axes and the color of plotted points correspond to reduced representation of 5-D crystallographic data along three directions that explain most variance in pairwise distance data (third dimension illustrated as depth in the colorbar). Colored lines schematically show ICC evolution during rolling. (For interpretation of the references to color in this figure legend, the reader is referred to the web version of this article.)

#### 4. Discussion

Our results demonstrate the importance of initial texture in determining the steady state texture and interface character during severe plastic deformation of Cu-Nb nano-laminates. The high strain interface characters observed in our atomistic simulations are consistent with existing experimental results. The ARB OR is the predominant interface character observed during ARB experiments for layer thicknesses above 30 nm [6,8]. Upon further deformation from 30 to 10 nm, the ARB Goss OR develops along twinned regions of the Cu layer [16]. These two ORs are the major driven steady states in four of the seven atomistic models tested in this work: ARB bicrystal 1 maintains the ARB OR over 90% of the interface, while ARB bicrystal 2, PVD bicrystal 2, and PVD seed model 2 all have interfaces with a majority ARB Goss OR associated with twinning in the Cu layer. PVD bicrystal 2 and seed model 2 pass through the ARB OR at intermediate layer thickness before reorientation to the ARB Goss OR.

(b)

In cross-rolled ARB, the sample is rotated by 90 deg. at a layer thickness of 60 nm before a final rolling pass. The ARB- $\alpha$  OR has been observed in cross rolled ARB composites with layer thickness 20 nm with a predominant Nb{001}<110> orientation [16]. Inter-

estingly, ARB- $\alpha$  is the major driven steady state in PVD seed model 1. Three pairs of models in this work can be viewed as cross rolled variants with interchanged TD and RD. Each has a distinct steady state texture, demonstrating that a change in strain path may also be viewed as an alteration of initial texture that directs texture evolution into a different basin of attraction.

One basin of attraction found in our models, ARB- $\gamma$ , has not previously been observed in experiments. Crystal plasticity simulations have shown that the ARB- $\gamma$  OR with a Nb {111}<110> end member is a plastically stable, driven steady state [6]. Our simulations show that the ARB- $\gamma$  OR dominates the texture of both PVD bicrystal 1 and the randomly textured model at high strains. As a hitherto unobserved, yet plastically stable OR, ARB- $\gamma$  represents a potential new class of ARB composites that may be experimentally obtainable by modifying initial composite texture [16]. Such plastically stable ORs may be obtained by seeding Cu-Nb nanocomposites with highly textured bilayers. The effect of these seed layers is shown as the attraction of diverse initial ICCs to distinct steady state ICCs in Fig. 5.

Our work suggests that seed layers play an important role in governing behavior in bulk polycrystalline layers during deformation. Both PVD seed models show extensive grain coalescence

during deformation and have different steady state textures. Seed crystals evidently pull grains in the layer interiors towards a plastically stable state that depends on seed layer texture. Such a biasing effect of the seed layer is consistent with the concept of an interface affected zone (IAZ) proposed by Mara et al. [28,38]. The IAZ is a region directly surrounding a heterophase interface which allows for selective local texturing due to interface mediated plasticity. Experimentally, the IAZ has typically been examined in systems with grain sizes much larger than those in our simulations (100 nm compared to 3-12 nm). Nevertheless, as layers are rolled down to sub-micron dimensions, IAZs from neighboring interfaces begin to overlap, dominating texture evolution in the entire layer. CPFE simulations that include an IAZ show that the IAZ tends to reduce the number plastically stable interfaces compared to interfaces with no IAZ [29–31]. Thus, it appears plausible that the emergence of distinct basins of attraction during rolling may be the outcome of a down-selection of plastically stable textures induced by IAZs.

In addition to the influence of initial textures on steady-state textures, our simulations also reveal a wealth of SPD-related phenomena, such as deformation-induced grain refinement and coalescence, grain boundary migration, and interfacial plasticity. Experiments on ultra-fine grained nanocrystalline metals also exhibit deformation mechanisms mediated by a combination of crystal and grain boundary plasticity [19,32,35,39]. Deformation-induced grain coalescence has been observed in ultra-fine grained Pd and Ni [33,36,37]. In these experiments, just as in our simulations, stacking faults are seen to cut and erode grain boundaries during mechanical coarsening. The interplay between plasticity of ultrafine grain structures and heterophase interfaces during SPD is largely unexplored territory. Our work suggests that a combination of atomistic simulations and quantitative crystal orientation analysis is an effective approach to advancing fundamental understanding of such processes.

There are several aspects of the microstructure of composites that are not captured in this work due to the limited model size. For example, the columnar grain structure of real PVD films is not included in our models. In ARB experiments, composites start off at millimeter thickness and the grain structure is refined to the nanoscale. Our simulations start with idealized nano-crystalline structures that do not include preexisting bulk defects or statistically stored interface defects. The small initial layer sizes in our simulations also preclude the observation of plastic flow instabilities such as shear banding and kinking. Nevertheless, we have shown that large scale molecular statics calculations of accumulative roll bonding of Cu-Nb nanocomposites can identify a variety of mechanisms that contribute to steady state textures that are consistent with experiments and crystal plasticity simulations.

## **Declaration of Competing Interest**

The authors declare no competing interests

#### **CRediT authorship contribution statement**

**Ian Chesser:** Investigation, Formal analysis, Writing - original draft. **Elizabeth A. Holm:** Supervision, Writing - review & editing. **Michael J. Demkowicz:** Methodology, Supervision, Writing - review & editing.

## Acknowledgments

Funding: The contribution of M. J. D. to this work was supported by the Department of Energy, National Nuclear Security Administration under Award no. DE-NA0003857. Computational resources were provided by the Texas A&M High Performance Research Computing program. The contribution of I.C. and E.A.H. to

this work was supported by National Science Foundation grants GFRP-1252522 and DMR-1710186, as well as the CMU CIT Seed Incubation Program. We are grateful to D. Farkas for providing atomistic models of polycrystalline Cu and polycrystalline Nb.

#### Supplementary materials

Supplementary material associated with this article can be found, in the online version, at doi:10.1016/j.actamat.2019.10.058.

#### References

- [1] U.Fred Kocks, et al., Texture and anisotropy: Preferred Orientations in Polycrystals and Their Effect On Materials Properties, Cambridge university press,
- [2] P.P. Bhattacharjee, R.K. Ray, A. Upadhyaya, Development of cube texture in pure Ni, Ni–W and Ni–Mo alloys prepared by the powder metallurgy route, Scr. Mate.r 53 (12) (2005) 1477–1481.
- [3] D. Barbier, et al., Analysis of the tensile behavior of a twip steel based on the texture and microstructure evolutions, Mater. Sci. Eng.: A 500 (1–2) (2009) 196–206.
- [4] I.L. Dillamore, W.T. Roberts, Rolling textures in fcc and bcc metals, Acta Metall. 12 (3) (1964) 281–293.
- [5] T.C. Lowe, R.Z. Valiev, Investigations and Applications of Severe Plastic Deformation, 80, Springer Science & Business Media, 2012.
- [6] I.J. Beyerlein, et al., Emergence of stable interfaces under extreme plastic deformation, Proc. Natl. Acad. Sci. 111 (12) (2014) 4386–4390.
- [7] T.G. Langdon, Twenty-five years of ultrafine-grained materials: achieving exceptional properties through grain refinement, Acta Mater. 61 (19) (2013) 7035–7059.
- [8] I.J. Beyerlein, et al., Defect-interface interactions, Prog. Mater. Sci. 74 (2015) 125–210.
- [9] I.J. Beyerlein, N.a. Mara, J. Wang, J.S. Carpenter, S.J. Zheng, W.Z. Han, T.M. Pollock, Structure-property-functionality of bimetal interfaces, JOM 64 (10) (2012) 1192–1207, doi:10.1007/s11837-012-0431-0.
- [10] I.J. Beyerlein, L.S. Tóth, Progress in materials science texture evolution in equalchannel angular extrusion, Prog. Mater. Sci. 54 (4) (2009) 427–510, doi:10. 1016/j.pmatsci.2009.01.001.
- [11] a. Misra, M.J. Demkowicz, X. Zhang, R.G. Hoagland, The radiation damage tolerance of ultra-high strength nanolayered composites, JOM 59 (9) (2007) 62–65, doi:10.1007/s11837-007-0120-6.
- [12] M.J. Demkowicz, L. Thilly, Structure, shear resistance and interaction with point defects of interfaces in cu-nb nanocomposites synthesized by severe plastic deformation, Acta Mater. 59 (20) (2011) 7744–7756, doi:10.1016/j. actamat.2011.09.004.
- [13] W. Han, M.J. Demkowicz, N.a. Mara, E. Fu, S. Sinha, A.D. Rollett, A. Misra, Design of radiation tolerant materials via interface engineering, Adv. Mater. 25 (48) (2013) 6975–6979, doi:10.1002/adma.201303400.
- [14] R. Valiev, Nanostructuring of metals by severe plastic deformation for advanced properties, Nat. Mater. 3 (8) (2004) 511–516 Retrieved from, doi:10.1038/nmat1180.
- [15] a. Misra, J.P. Hirth, R.G. Hoagland, J.D. Embury, H. Kung, Dislocation mechanisms and symmetric slip in rolled nano-scale metallic multilayers, Acta Mater. 52 (8) (2004) 2387–2394, doi:10.1016/j.actamat.2004.01.029.
- [16] N.a. Mara, I.J. Beyerlein, Review: effect of bimetal interface structure on the mechanical behavior of cu-nb fcc-bcc nanolayered composites, J. Mater. Sci. 49 (19) (2014) 6497–6516, doi:10.1007/s10853-014-8342-9.
- [17] Y.T. Zhu, X.Z. Liao, X.L. Wu, Deformation twinning in nanocrystalline materials, Prog. Mater. Sci. 57 (1) (2012) 1–62, doi:10.1016/j.pmatsci.2011.05.001.
- [18] Derek Hull, J David, Bacon, Introduction to Dislocations, Butterworth-Heinemann, 2001.
- [19] Y. Zhang, G.J. Tucker, J.R. Trelewicz, Acta materialia stress-assisted grain growth in nanocrystalline metals: grain boundary mediated mechanisms and stabilization through alloying, Acta Mater. 131 (2017) 39–47, doi:10.1016/j.actamat. 2017.03.060
- [20] O.G. Vinogradov, On reliability of molecular statics simulations of plasticity in crystals, Comput. Mater. Sci. 50 (2) (2010) 771–775, doi:10.1016/j.commatsci. 2010.10.009.
- [21] D. Farkas, A. Frøseth, H.V. Swygenhoven, Grain boundary migration during room temperature deformation of nanocrystalline Ni, Scr Mater. 55 (8) (2006) 695–698.
- [22] P.M. Larsen, S. Schmidt, J. Schiøtz, Robust structural identification via polyhedral template matching, Model. Simul. Mater. Sci. Eng. 24 (5) (2016) 055007.
- [23] A. Stukowski, Structure identification methods for atomistic simulations of crystalline materials, Model. Simul. Mater. Sci. Eng. 20 (2012) 45021, doi:10. 1088/0965-0393/20/4/045021.
- [24] T. Francis, et al., A geodesic octonion metric for grain boundaries, Acta Mater. 166 (2019) 135–147.
- [25] T.F. Cox, M.AA Cox, Multidimensional Scaling, Chapman and hall/CRC, 2000.
- [26] K. Verbeken, L. Barbé, D. Raabe, Evaluation of the crystallographic orientation relationships between fcc and bcc phases in trip steels, ISIJ Int. 49 (10) (2009) 1601–1609, doi:10.2355/isijinternational.49.1601.

- [27] S.B. Lee, J.E. Ledonne, S.C.V. Lim, I.J. Beyerlein, A.D. Rollett, The heterophase interface character distribution of physical vapor-deposited and accumulative roll-bonded cu-nb multilayer composites, Acta Mater. 60 (4) (2012) 1747–1761, doi:10.1016/j.actamat.2011.12.007.
- [28] J.S. Carpenter, et al., Interface-Driven plasticity: the presence of an interface affected zone in metallic lamellar composites, Adv. Eng. Mater 17 (1) (2015) 109–114.
- [29] J.R. Mayeur, et al., Incorporating interface affected zones into crystal plasticity, Int. I, Plast. 65 (2015) 206–225.
- [30] J.R. Mayeur, I.J. Beyerlein, C.a. Bronkhorst, H.M. Mourad, B.L. Hansen, A crystal plasticity study of heterophase interface character stability of Cu/Nb bicrystals, Int. J. Plast. 48 (2013) 72–91, doi:10.1016/j.ijplas.2013.02.006.
- [31] J. Mayeur, et al., The influence of grain interactions on the plastic stability of heterophase interfaces, Materials (Basel) 7 (1) (2014) 302–322.
- [32] J. Hu, et al., Grain boundary stability governs hardening and softening in extremely fine nanograined metals, Science 355 (6331) (2017) 1292–1296.
- [33] Z. Shan, et al., Grain boundary-mediated plasticity in nanocrystalline nickel, Science 305 (5684) (2004) 654–657.
- [34] M.J. Demkowicz, J. Wang, R.G. Hoagland, Interfaces Between Dissimilar Crystalline Solids, Dislocation in Solids, Volume 14: A Tribute to Hirth JP, F.R.N. Nabarro (Ed.), Elsevier, Amsterdam, 2008.
- [35] A.J. Vattré, et al., Computational design of patterned interfaces using reduced order models, Sci. Rep. 4 (2014) 6231.

- [36] L. Wang, et al., Grain rotation mediated by grain boundary dislocations in nanocrystalline platinum, Nat. Commun. 5 (2014) 4402.
- [37] R. Hull, J.M. Gibson, L.E. Brus, D.J. Norris, M.G. Bawendi, A. Zunger, M.F. Thorpe, (2004). Grain boundary – Mediated Plasticity in nanocrystalline nickel, 305(July), 654–658.
- [38] J. Mayeur, et al., The influence of grain interactions on the plastic stability of heterophase interfaces, Materials (Basel) 7 (1) (2014) 302–322.
- [39] J.R. Mayeur, I.J. Beyerlein, C.a. Bronkhorst, H.M. Mourad, B.L. Hansen, A crystal plasticity study of heterophase interface character stability of Cu/Nb bicrystals, Int. J. Plast. 48 (2013) 72–91, doi:10.1016/j.ijplas.2013.02.006.
- [40] M.J. Demkowicz, R.G. Hoagland, Structure of Kurdjumov-Sachs interfaces in simulations of a copper-niobium bilayer, J. Nucl. Mater. 372 (1) (2008) 45–52, doi:10.1016/j.jnucmat.2007.02.001.
- [41] G. Kurdjumow, G. Sachs, Über den mechanismus der stahlhärtung, Zeitschrift für Physik 64 (5–6) (1930) 325–343.
- [42] M.J. Demkowicz, R.G. Hoagland, Simulations of collision cascades in Cu-Nb layered composites using an eam interatomic potential, Int. J Appl. Mech. 1 (03) (2009) 421–442.
- [43] J. Wang, K. Kang, R.F. Zhang, S.J. Zheng, I.J. Beyerlein, N.a. Mara, Structure and property of interfaces in Arb Cu/Nb laminated composites, JOM 64 (10) (2012) 1208–1217, doi:10.1007/s11837-012-0429-7.
- [44] I. Chesser, et al., Learning the grain boundary manifold: tools for visualizing and fitting grain boundary properties, 2019. Available at SSRN 3460311.